Title

- **De novo synthesis and salvage pathway coordinately regulates polyamine homeostasis and determines T cell proliferation and function.**
- **Polyamine homeostasis determines T cell function.**

Authors

Ruohan Wu[1†], Xuyong Chen[1†], Siwen Kang[1†], Tingting Wang[1], JN Rashida Gnanaprakasam[1], Yufeng Yao[3], Lingling Liu[1], Song Guo Zheng[2], Gaofeng Fan[3], Mark R Burns[4] and Ruoning Wang[1]*

Affiliations

[1]Center for Childhood Cancer & Blood Diseases, Hematology/Oncology & BMT, Abigail Wexner Research Institute at Nationwide Children's Hospital, The Ohio State University, Columbus, OH, USA.

[2]Division of Rheumatology and Immunology, Department of Internal Medicine at Ohio State University of Medicine and Wexner Medical Center, Columbus, OH, USA.

[3]School of Life Science and Technology, ShanghaiTech University, Shanghai, China.

[4]Aminex Therapeutics Inc., Epsom, NH 03234, USA.

†Wu R, Chen X and Kang S contributed equally to this paper

*Correspondence should be addressed to:

Ruoning Wang, Phone: 614-335-2980; Fax: 614-722-5895.
ruoning.wang@nationwidechildrens.org;

Abstract

Robust and effective T cell-mediated immune responses require proper allocation of metabolic resources through metabolic pathways to sustain the energetically costly immune response. As an essential class of polycationic metabolites ubiquitously present in all living organisms, the polyamine pool is tightly regulated by biosynthesis and salvage pathway. We demonstrated that arginine is a major carbon donor and glutamine is a minor carbon donor for polyamine biosynthesis in T cells. Accordingly, the dependence of T cells can be partially relieved by replenishing the polyamine pool. In response to the blockage of de novo synthesis, T cells can rapidly restore the polyamine pool through a compensatory increase in polyamine uptake from the environment, indicating a layer of metabolic plasticity. Simultaneously blocking synthesis and uptake depletes the intracellular PA pool, inhibits T cell proliferation, suppresses T cell inflammation, indicating the potential therapeutic value of targeting the polyamine for managing inflammatory and autoimmune diseases.

MAIN TEXT

Introduction

48 To cope with pathogens' capacity for exponential growth, T cells have evolved mechanisms for
49 rapidly adjusting their metabolism in response to T cell receptor (TCR) activation and additional
50 signals indicating environmental change. A robust and effective metabolic reprogramming enables
51 T cells to rapidly expand in number and differentiate to achieve large numbers of effector cells
52 specialized in producing high levels of cytokines. Emerging evidences have shown that metabolic
53 rewiring of the central carbon metabolism maximizes the acquisition and assimilation of energy
54 and carbon, and prepare T cells for growth, differentiation, immune regulation and defense (*1-7*).
55 Glycolysis, the pentose phosphate pathway (PPP), the Krebs cycle and fatty acid oxidation (FAO)
56 represent a core set of metabolic pathways that transform carbon and chemical energy from
57 environmental nutrients to support the bioenergetic and biosynthesis needs of T cells. Beyond that,
58 a myriad of peripheral metabolic pathways is integrated to complex metabolic networks and are
59 tightly regulated to generate specialized metabolites, which are essential for maintaining
60 homeostasis and immune functions of T cells.
61
62 Non-essential amino acids including arginine, glutamine, and proline have both anabolic and
63 catabolic functions, providing building blocks for protein and connecting central carbon
64 metabolism to a variety of specialized metabolism, including polyamine biosynthesis (*8-13*).
65 Polyamine is an essential class of polycationic metabolites ubiquitously present in all living
66 organisms. In addition to de novo biosynthesis, other metabolic routes including polyamine
67 catabolism, influx and efflux act in concert to determine the size of the intracellular polyamine pool
68 (*14, 15*). Disrupting polyamine homeostasis can affect a plethora of cellular processes, including
69 transcription, translation, redox balance, and mitochondria quality control (*16-18*). Dysregulation
70 of the level of polyamine and its amino acid precursors has been found to be associated with
71 inflammation and autoimmune diseases (*18-23*). We have previously reported that polyamine is
72 one of the most upregulated metabolite groups following T cell activation, and transcription factor

73 MYC is responsible for its upregulation (*24*). Emerging evidence have also shown that polyamine
74 homeostasis is tightly regulated in cellular contexts other than T cells, which have critical roles in
75 immune regulation and defense (*23-30*). As such, a better understanding of how polyamine
76 homeostasis is regulated in immune cells will reveal the fundamental principles of the emerging
77 connections between immune cell metabolic fitness and functional robustness. Further knowledge
78 will also enable us to devise rational and practical approaches to treat inflammatory and
79 autoimmune diseases.
80
81 Intrinsic T cell signaling cascades are instrumental in the control of T cell metabolic programming
82 (*31-36*). Numerous extrinsic environmental factors including oxygen and nutrient supplies also
83 significantly influence T cell metabolic phenotypes and, thus, immune functions *in vivo* (*3, 37*).
84 Here, we report that the intracellular polyamine pool is tightly regulated by de novo biosynthesis
85 and salvage, through the import of extracellular polyamine. Heightened arginine and glutamine
86 catabolism provide carbon sources to support polyamine de novo biosynthesis *in vitro*. Genetic and
87 pharmacologic ablation of de novo biosynthesis of polyamine is sufficient to deplete the polyamine
88 pool and suppress T cell proliferation *in vitro*. However, de novo biosynthesis is dispensable in
89 driving T cell proliferation *in vivo* where T cells can salvage circulating polyamine to maintain
90 intracellular polyamine pool. Simultaneously blocking polyamine synthesis and salvage inhibits T
91 cell proliferation *in vivo* and confers protection against the pathogenic development of experimental
92 autoimmune encephalomyelitis (EAE). Our findings implicate the potential therapeutic value of
93 targeting the polyamine metabolism in treating and managing inflammatory and autoimmune
94 diseases.

Results

Inhibition of ODC reduces T cell proliferation and viability *in vitro*

We previously reported that a Myc-dependent non-canonical metabolic pathway links amino acid catabolism to the biosynthesis of polyamine during T cell activation (*38*). To investigate the role of polyamine metabolism in T cells, we employed a genetic and a pharmacologic approach to ablate polyamine de novo biosynthesis. Since ornithine decarboxylase (ODC), the rate-limiting enzyme in polyamine de novo biosynthetic pathway, is essential for early embryo development, and ODC germline knockout is embryonically lethal (*39*), we obtained a mouse strain containing a reporter-tagged conditional allele of ODC (FRT-LacZ; ODC^{fl}) generated by the European Mouse Mutant Archive (*40*). We first crossed this strain with the FLP knock-in mouse strain, which removed the LacZ-reporter allele and generated the strain containing the conditional allele (ODC^{fl}). Then, we generated a T cell-specific ODC knockout strain (ODC cKO) by crossing the ODC^{fl} strain with the CD4-Cre strain. The deletion of ODC was validated by qPCR (Fig. S1A), and the ablation of polyamine de novo synthesis was further validated by the accumulation of ornithine (substrate of ODC) and the depletion of spermine, spermidine, putrescine and N-Acetylputrescine (Fig. S1B). ODC deletion did not affect the distribution of T cell subsets in the thymus, spleen and lymph nodes (Fig. S2A and S2B). In addition, the percentage of naturally occurring IFN-γ-producing, IL-17-producing, and $FoxP3^{+}$ CD4 T cells is comparable in both WT and ODC cKO animals (Fig. S2C). However, genetic deletion of ODC significantly delayed cell cycle progression from G0/G1 to the S phase after T cell activation and suppressed overall T cell proliferation in vitro (Fig. 1A and 1B). Consistent with the impact of genetic deletion of ODC on T cells, difluoromethylornithine (DFMO), a potent inhibitor of ODC, inhibited activation-induced T cell cycle progression and proliferation in vitro (Fig. 1C and 1D). Finally, both genetic deletion of ODC and DFMO treatment

119 caused moderately more cell death after activation in a time-dependent manner (Fig. 1E and 1F).
120 Together, our results indicate that polyamine homeostasis is critical for T cell proliferation and
121 survival.
122

123 **ODC activity is dispensable for T cell proliferation and function *in vivo***

124 Controlling polyamine homeostasis is crucial for supporting cellular functions in all cell types, and
125 both de novo biosynthesis and salvage by importing extracellular polyamine into the cell tightly
126 regulates cellular polyamine-pool size (*16-18*). Without exogenous polyamine supplements in cell
127 culture media, we envisioned that T cells would solely depend on de novo biosynthesis to maintain
128 the intracellular polyamine pool *in vitro*. However, circulating polyamines that are provided by
129 dietary intake and by intestinal microbiota may be a source of exogenous polyamine for T cells *in*
130 *vivo* (*15, 41*). To assess the impact of ablating de novo biosynthesis on CD4 T cell proliferation *in*
131 *vivo*, we employed a well-established competitive homeostatic proliferation assay to determine the
132 ratio and carboxyfluorescein succinimidyl ester (CFSE) dilution pattern of purified *WT(Thy1.1$^+$)*
133 or *ODC$^{-/-}$(Thy1.2$^+$)* CD4$^+$ T cells in Rag1-deficient mice. Surprisingly, the ratio between *WT* and
134 *ODC$^{-/-}$* CD4$^+$ T cells was similar before and after adoptive transfer. Additionally, *WT* and *ODC$^{-/-}$*
135 CD4$^+$ T cells display an overlapped CFSE dilution pattern, indicating that the loss of ODC did not
136 affect T cell proliferation *in vivo* (Fig. 2A). Next, we sought to measure antigen-specific, TCR-
137 dependent proliferation of *WT* or *ODC$^{-/-}$* CD4$^+$ T cells. We crossed Thy1.1 and CD4-Cre, ODC^{fl}
138 mice with OT-II transgenic mice to generate *WT(Thy1.1$^+$)* and *ODC$^{-/-}$(Thy1.2$^+$)* donor OT-II
139 strains in CD45.2$^+$ background. We then adoptively transferred mixed and CFSE labelled *WT* and
140 *ODC$^{-/-}$* CD4$^+$ T cells into CD45.1$^+$ mice that were immunized with chicken ovalbumin 323-339
141 peptide (OVA$_{323-339}$) in complete Freund's adjuvant (CFA). After 7 days, we measured the
142 percentage ratio and CFSE dilution pattern of *WT(Thy1.1$^+$)* and *ODC$^{-/-}$(Thy1.2$^+$)* CD4$^+$ T cells in
143 popliteal lymph node. Consistent with the homeostatic proliferation results, *WT* and *ODC$^{-/-}$* OT-II

144 specific $CD4^+$ T cells display a comparable antigen-specific proliferation (Fig. 2B). The expansion
145 and balance between pro-inflammatory $CD4^+$ T effector (T_{eff}) cells determine the pathogenic
146 development of experimental autoimmune encephalomyelitis (EAE), a murine model of multiple
147 sclerosis (MS), which is an inflammatory demyelinating disease of the central nervous system
148 (CNS). We employed this well-characterized system to further interrogate an *in vivo* CD4 T cell
149 response in the absence of polyamine de novo biosynthesis. In line with our homeostatic and
150 antigen-specific proliferation data, neither the genetic deletion of ODC in T cells nor the systemic
151 delivery of DFMO changes the kinetics of pathogenic progression (Fig. 2C and 2D). Together, our
152 data indicates that polyamine salvage from circulation may be able to support T cell proliferation
153 and effector function by compensating for the loss of de novo biosynthesis in the in vivo
154 environment.
155

156 **Polyamine salvage compensates for the loss of biosynthesis activity *in vitro***

157 Next, we investigated the role of polyamine salvage (uptake) in regulating polyamine homeostasis
158 in T cell. We measured polyamine uptake activity using radioactive-labelled putrescine (^{14}C-
159 Putrescine) in naïve, active *WT* and $ODC^{-/-}$ T cells. Active T cells displayed higher polyamine
160 uptake activity than naïve T cells (Fig. 3A). Importantly, ablation of ODC induces a compensatory
161 increase in polyamine uptake (Fig. 3B). Next, we asked if polyamine uptake is sufficient to maintain
162 polyamine homeostasis and support T cell proliferation in the absence of ODC activity. While
163 genetic deletion or pharmacologic inhibition of ODC significantly delayed cell cycle progression
164 from G0/G1 to the S phase and suppressed overall T cell proliferation, exogenous polyamine
165 supplement could restore the cell cycle progression, proliferation and viability in DMFO-treated
166 and $ODC^{-/-}$ $CD4^+$ T cells *in vitro* (Fig. 3C-3F and Fig. S3A-S3B). We then sought to employ a
167 pharmacologic approach to block polyamine uptake and assessed the role of polyamine uptake in
168 regulating polyamine homeostasis. AMXT 1501 (AMXT) is a novel lipophilic polyamine mimetic

169 that potently blocks polyamine uptake in the low nanomolar concentration (*42*). The combination
170 of AMXT and DFMO could effectively deplete the polyamine pool in tumor cells and suppress the
171 growth of tumors in various animal models (*43-45*). These promising preclinical studies led to a
172 recently opened Phase I clinical trial in solid tumors (NCT03077477). Similar to the genetic data
173 (Fig. 3B), DFMO treatment induces a compensatory increase in polyamine uptake, which can be
174 blocked by AMXT 1501 (Fig. 3G). In addition, AMXT 1501 could significantly suppresses
175 exogenous polyamine-mediated cell proliferation and viability in *ODC*$^{-/-}$, but not *WT* CD4^{+} T cells
176 (Fig. 3H and S3C), indicating that either polyamine salvage or biosynthesis is sufficient to maintain
177 polyamine homeostasis in T cells. Supporting this idea, AMXT 1501 treatment alone failed to
178 suppress T cell homeostatic proliferation or antigen-specific proliferation (Fig. S4A and S4B).
179 These results, together with the results described above, suggest that the salvage pathway and the
180 de novo biosynthesis pathway can compensate for the loss of each other, representing a layer of
181 metabolic plasticity engaged by T cells to maintain polyamine homeostasis.
182

183 **Simultaneously blocking polyamine salvage and biosynthesis suppresses T cell proliferation**
184 ***in vivo***

185 Given that either genetically ablating ODC or pharmacologically blocking polyamine uptake failed
186 to impact T cell proliferation and function *in vivo*, we sought to assess the impacts of simultaneously
187 blocking polyamine salvage and biosynthesis on T cells *in vivo*. We employed competitive
188 homeostatic proliferation and antigen-specific T cell proliferation assays to determine the
189 proliferation of *WT* and *ODC*$^{-/-}$ donor CD4^{+} T cells in recipient mice, which were treated with
190 vehicle or AMXT 1501 during the course of experiment. Donor *ODC*$^{-/-}$ CD4^{+} T cells recovered
191 from AMXT 1501 treated animals but not from vehicle treated animals displayed reduced
192 percentage and delayed proliferation compared with competitive *WT* CD4^{+} T cells (Fig. 4A and
193 4B). We then sought to assess the impacts of simultaneously blocking polyamine salvage and

194 biosynthesis on T cells in the EAE model. The genetic deletion of ODC in T cells failed to cause
195 any significant changes in EAE pathogenic progression. Animals that were treated with AMXT
196 1501 displayed a delayed disease onset initially, but eventually proceeded with pathologic
197 development and reached the endpoint. Importantly, the combination of AMXT 1501 with genetic
198 deletion of ODC in T cells conferred full protection against EAE pathogenic progression (Fig. 4C).
199 ODC inhibitor DFMO is an FDA-approved medicine for hirsutism and African sleeping sickness
200 and has been widely tested as a chemopreventive and chemotherapeutic agent against solid tumors
201 (*46-51*). Similar to the genetic data, DFMO alone failed to suppress EAE pathogenic progression
202 (Fig. 4D). Although AMXT alone was sufficient to delay EAE onset moderately, it failed to protect
203 animals from reaching the endpoint (Fig. 4D). We envision that the combination of DFMO and
204 AMXT may be sufficient to deplete T cell polyamine pool, and consequently suppress T cell
205 proliferation and effector function *in vivo*. Supporting this idea, the combination of AMXT and
206 DMFO, but not single treatments, conferred full protection against EAE pathogenic progression
207 (Fig. 4D). Inflammatory T_H1, T_H17, and FoxP3-expressing regulatory T cells (T_{reg}) are closely
208 related to CD4 T cell subsets but with distinct functions. The balance between pro-inflammatory
209 $CD4^+$ T_{eff} cells and T_{reg} cells determines the pathogenic development of EAE. Next, we examined
210 the polyamine's role in CD4 T_{eff} cell differentiation *in vitro*. Without exogenous polyamine
211 supplemented in cell culture media, maintenance of the intracellular polyamine pool depends solely
212 on ODC-mediated polyamine biosynthesis. Remarkably, intracellular polyamine depletion
213 resulting from ODC deficiency inhibited pro-inflammatory T_H1 and T_H17 cell differentiation while
214 enhancing anti-inflammatory iT_{reg} cell differentiation in vitro (Fig. S5). Together, our results
215 indicate that the polyamine blocking approach, via ablation of salvage and biosynthesis pathways,
216 suppresses T cell proliferation and may be a potential new therapy for treating inflammatory and
217 autoimmune disease.
218

219 **Amino acid catabolism provides carbon sources for polyamine biosynthesis**

220 Dietary intake and intestinal microbiota metabolism are major sources of circulating polyamine
221 (*15, 41*). We reasoned that an understanding of carbon sources that drive polyamine biosynthesis
222 in T cells would enable the development of nutritional approaches for effectively controlling
223 polyamine homeostasis in T cells. While arginine catabolism is integrated into the urea cycle to
224 detoxify ammonia and provides the precursor for polyamine biosynthesis, we previously reported
225 that glutamine-derived carbon could be funneled into polyamine biosynthesis through ornithine in
226 T cells (*24*). In addition, proline can also provide carbon for polyamine biosynthesis in the placenta
227 and in plants (*13, 52*). To determine to what extent these three amino acids contribute to polyamine
228 biosynthesis, we applied the stable isotope of carbon-13 (^{13}C) labeling and mass spectrometry
229 approach. We supplied $^{13}C_6$-Arginine, $^{13}C_5$-Glutamine, or $^{13}C_5$-Proline as metabolic tracers in T cell
230 culture media and then followed ^{13}C incorporation into individual metabolites (Fig. 5A). While not
231 all desired metabolites were detected in our experiment due to technical limitation and a portion of
232 proline was produced through de novo biosynthesis, our results clearly demonstrated that $^{13}C_5$-
233 Proline only contributes a minimal amount of $^{13}C_5$ isotopologue of ornithine and polyamine (Fig.
234 5B). In contrast, $^{13}C_6$-Arginine and $^{13}C_5$-Glutamine contribute 50% and 40% of $^{13}C_5$-Ornithine,
235 respectively (Fig. 5B). Importantly, $^{13}C_6$-Arginine and $^{13}C_5$-Glutamine contribute around 80% and
236 20% of $^{13}C_4$ isotopologues of polyamine (putrescine and spermidine generated via decarboxylation
237 of ornithine), respectively (Fig. 5B). Thus, we conclude that arginine is a major carbon donor and
238 glutamine is a minor carbon donor for supporting polyamine biosynthesis in T cells *in vitro*.

239

240 **Arginine catabolism drives T cell proliferation partially through supporting polyamine**
241 **biosynthesis**

242

While arginine is generally considered a non-essential amino acid, T cells are arginine auxotrophic *in vitro* (*29, 53, 54*). Arginine is required to maintain $CD4^+$ T cells viability, driving proliferative and proinflammatory lineage (T_H17) differentiation (Fig. 5C and 5D). While the amount of most amino acids is in the low micromolar (μM) range, the concentration of arginine is in the millimolar (mM) range in cell culture media. We envisioned that, in addition to a general requirement of arginine for protein synthesis, arginine might also support T cell proliferation and differentiation through polyamine biosynthesis. To test this idea, we titrated down the amount of arginine in cell culture media and found that 10 μM of arginine was sufficient to support protein synthesis and the growth of cell mass at the early time point after T cell activation but failed to maintain cell viability and drive proliferation later (Fig. S6A and 5E). We envision that arginine supports protein synthesis and polyamine biosynthesis, both of which are required to drive T cell proliferation. Supporting this idea, we have shown that a low level of arginine (10 μM) in culture media is sufficient to support protein synthesis, but not proliferation (Fig. 5E). Similar to what we found in polyamine depletion condition (Fig. S5), low level of arginine in culture media reduces T_H17 differentiation (Fig. 5E). However, polyamine supplements can partially restore T cell proliferation and T_H17 differentiation with a low level of arginine (10 μM) (Fig. S6C). In contrast, polyamine supplements failed to restore T cell proliferation and differentiation under arginine starvation condition (0 μM) (Fig. S6B). Collectively, our data indicate that T cell activation engages a metabolic axis that connects arginine catabolism to polyamine de novo biosynthesis.

Discussion

Fast-growing pathogens impose selective pressures on the metabolic fitness and metabolic plasticity of host immune cells, which are necessary for immune cells to maintain homeostasis

268 while remaining ready to mount rapid responses under diverse metabolic and immune conditions
269 (*3, 55-58*). A robust T cell-mediated adaptive immune response exhibits high and dynamic
270 metabolic demands in T cells, which is accommodated through fine-tuned regulation on both the
271 central carbon metabolic pathways, and peripheral metabolic pathways including polyamine
272 metabolism (*38, 59-65*). The standard formulation of cell culture media, which does not fully
273 recapitulate the physiological metabolite composition in the plasma and tissue microenvironment,
274 often leads to a significant metabolic adaptation of growing cells *in vitro*. Metabolic phenotypes of
275 cells growing *in vivo* may further differ from cells growing *in vitro* as a result of other
276 environmental factors including oxygen level, cellular competition and cooperation, and the
277 biophysical properties of the extracellular matrix (*66-71*). Similarly, T cell metabolism can respond
278 and adapt to environmental nutrient levels (*3, 37*). Our studies revealed T cells' capacity to engage
279 in both de novo biosynthetic and salvage pathways to fine-tune polyamine homeostasis, which is
280 required to maximize metabolic fitness and optimize CD4 T_{eff} cell proliferation and differentiation.
281 Such metabolic plasticity is likely to be crucial for T cells' ability to elicit robust immune responses
282 in different tissue contexts.
283
284 Glutamine and arginine are two non-essential amino acids that not only fulfill the general
285 requirements for protein synthesis, but also connect central carbon metabolism to a variety of
286 biosynthetic pathways to produce specialized metabolites (*22, 72-75*). Glutamine catabolism
287 funnels the anaplerotic flux of carbon into the TCA cycle and also provides sources of nitrogen and
288 carbon to support biosynthesis of nonessential amino acids, lipids, nucleotides, glutathione and
289 polyamines in T cells (*24, 38, 76-79*). Similarly, arginine is critical for maintaining T cells viability,
290 driving proliferative and effector functions (*25, 29, 54, 80*). We found that polyamine supplement
291 could partially relieve T cell's dependence on arginine, indicating that a key role of arginine
292 catabolism in T cells is to support polyamine biosynthesis. Consistently, arginine serves as a major

293 donor of carbon in polyamine biosynthesis, while glutamine only plays a minor role in funneling
294 carbon into polyamine in the presence of arginine in vitro. Interestingly, these two amino acids
295 contribute a comparable portion of carbon to ornithine, the precursor of polyamine. This finding is
296 in line with previous studies showing that arginine-derived ornithine is not the only source for
297 endogenous ornithine in most mammalian tissues (*81, 82*). In addition, our findings may implicate
298 ornithine as an important metabolic node representing a key branch point in both glutamine and
299 arginine catabolic pathways. Ornithine can be committed towards the urea cycle, proline
300 biosynthesis or de novo synthesis of polyamine. The production of ornithine from two different
301 metabolic precursors, glutamine and arginine, also enables fine-tuned coordination between the
302 metabolic flux shunted towards polyamine synthesis and the metabolic flux shunted towards other
303 specialized metabolites. Consistent with this idea, the overall high consumption rate of glutamine
304 and arginine may provide a sensitive and precise regulation on intermediate metabolites that can be
305 committed toward several metabolic branches, hence permitting rapid responses to meet the
306 metabolic demands of cell growth and cytokine production.
307
308 Active T cells and other highly proliferative cells such as tumor cells share metabolic characteristics
309 and are strictly dependent on the catabolism of glucose and glutamine through the central carbon
310 metabolic pathways (*83-90*). Similarly, elevated levels of polyamine are associated with T cell
311 activation and cell transformation (*24, 91, 92*). Importantly, pharmacologic or genetic targeting of
312 ODC, a transcriptional target of proto-oncogene MYC, could delay the development and the
313 progression of MYC-driven tumors in mice (*93, 94*). While pharmacologic agents targeting
314 polyamines such as the ODC inhibitor DFMO has generally low toxicity, DFMO yields only very
315 marginal therapeutic benefits in cancer patients as a single-agent therapy in clinical trials (*50*).
316 Clearly, cancer cells are capable of importing polyamine from circulation to overcome the effect of
317 DFMO. Supporting this idea, the simultaneous blockage of polyamine biosynthesis and uptake has

318 generated promising results in tumor preclinical animal models (*43, 45*). Mammalian cells can
319 uptake polyamine through endocytosis and membrane transport system mediated by several solute
320 carrier transporters (*95-99*). AMXT 1501 is a novel lipophilic polyamine mimetic that potently
321 blocks polyamine uptake through competing with polyamine (*42*). The combination of AMXT 1501
322 and DFMO could effectively deplete the polyamine pool in tumor cells and suppress the growth of
323 tumors in various animal models (*43-45*). These promising preclinical studies led to a recently
324 opened Phase I clinical trial in solid tumors (NCT03077477). Similarly, we have shown that ODC^{-}
325 $^{/-}$ $CD4^{+}$ T cells proliferate and function normal *in vivo*. However, concurrent treatment of $ODC^{-/-}$
326 $CD4^{+}$ T cells with AMXT 1501 abrogate their proliferation and inflammatory function *in vivo*.
327 Moreover, the combination of AMXT 1501 and DFMO could confer full protection to mice against
328 pathogenic development of EAE. Thus, polyamine blocking strategy via simultaneous blockade of
329 polyamine biosynthesis and salvage may present a promising and novel therapy for treating
330 inflammatory and autoimmune diseases.
331
332
333 **Materials and Methods**
334
335 **Mice**
336 C57BL/6NHsd (WT) mice, Rag-/- mice, OTII mice, Thy 1.1+ mice, and CD45.1+ mice were
337 obtained from Jackson laboratory (Bar Harbor, ME). CD4-Cre, ODC^{fl} (ODC cKO) mice with
338 C57BL/6 background were produced by FRT-LacZ; ODC^{fl} mice (European Mouse Mutant
339 Archive) crossed with the FLP knock-in mouse strain to remove the LacZ-reporter allele, and the
340 generated mouse strain containing the conditional allele (ODC^{fl}) was further crossed with the CD4-
341 Cre strain. For experiments, gender and age matched mice around 6-12 weeks of age kept in specific
342 pathogen-free conditions were used. All animal experiment protocols were approved by the

343 Institutional Animal Care and Use Committee of Abigail Wexner Research Institute at Nationwide
344 Children's Hospital (IACUC; protocol number AR13-00055).

345 **Flow cytometry**

346 For analysis of surface markers, cells were stained in PBS containing 2% (w/v) BSA and the
347 appropriate antibodies from Biolegend. Foxp3 expression was performed using the Foxp3 staining
348 kit from eBioscience. For intracellular cytokine IFN-ɣ and IL-17A staining, T cells were stimulated
349 for 4 hours with phorbol 12-myristate 13-acetate (PMA) and ionomycin in the presence of monensin
350 before being stained with CD4 antibody. Cells were then fixed and permeabilized using Foxp3
351 Fixation/Permeabilization solution according to the manufacturer's instructions (eBioscience™).
352 Cell total protein level was assessed by intracellular FITC (Fisher scientific) staining. Cell
353 proliferation was assessed by CFSE staining per the manufacturer's instructions (Invitrogen). Cell
354 viability was assessed by 7-AAD staining per the manufacturer's instructions (Biolegend). Flow
355 cytometry data were acquired on Novocyte (ACEA Biosciences) and were analyzed with FlowJo
356 software (TreeStar).

357 **Cell Culture**

358 For *in vitro* culture, total T cells or naïve CD4+ T cells were isolated from mouse spleen and lymph
359 nodes using MojoSort mouse CD3/CD4 naïve T cell Isolation Kit (Biolegend) following the
360 manufacturer's instructions. For all *in vitro* cell culture, unless indicated separately, complete
361 RPMI-1640 medium (containing 10% (v/v) heat-inactivated dialyzed fetal bovine serum (DFBS),
362 2 mM L-glutamine, 0.05 mM 2-mercaptoethanol, 100 units/mL penicillin, and 100 μg/mL
363 streptomycin) was used. DFBS was made by dialyzing against 100 volumes of PBS (five changes
364 in three days) using Slide-ALyzerTM G2 dialysis cassettes with cut-through MW size 2K
365 (ThermoFisher Scientific) at 4 ºC to remove any potential polyamines in the FBS. For the activation
366 assay, freshly isolated total T cells were either maintained in culture media with 5 ng/mL IL-7 for

367 resting state or were activated with 5 ng/mL IL-2 and plate-bound anti-CD3 (clone 145-2C11) and
368 anti-CD28 (clone 37.51). Plates were pre-coated with 2 μg/mL antibodies overnight at 4°C. Cells
369 were seeded as 1 X 10^6 cells/mL and cultured in RPMI 1640 media at 37 °C in 5% CO_2. For CFSE
370 dilution analysis, cells were pre-incubated for 10 min in 4 μM CFSE (Invitrogen) in PBS plus 5%
371 FBS before culture. For induced T_{reg} cell differentiation, 0.5 x10^6 naïve CD4+ T cells were cultured
372 with 200 U/mL IL-2, and 5 ng/mL TGF-β in 0.5 mL RPMI-1640 media in a 48-well tissue culture
373 plate that was pre-coated with 10 μg/mL anti-CD3 and 10 μg/mL anti-CD28 overnight at 4°C. For
374 T_H17 differentiation condition, 0.5 x10^6 naïve CD4+ T cells were seeded in each well pre-coated
375 with 10 μg/mL anti-CD3 and 10 μg/mL anti-CD28 overnight at 4°C and cultured with 8 μg/mL
376 anti–IL-2, 8 μg/mL anti–IL-4, 8 μg/mL anti–IFN-γ, 2 ng/mL TGF-β, and 20-50 ng/mL IL-6 in
377 0.5mL RPMI-1640 media in a 48-well tissue culture plate. For T_H1 differentiation condition, 0.5
378 x10^6 naïve CD4+ T cells were seeded in a well pre-coated with 10 μg/mL anti-CD3 and 10 μg/mL
379 anti-CD28 overnight at 4°C and cultured with 5 ng/mL IL-12, 10 μg/mL anti–IL-4, and 200 U/mL
380 IL-2 in 0.5mL RPMI-1640 media in a 48-well tissue culture plate for 72 hours. For invitro, cell
381 culture experiments, ODC inhibitor DFMO (Carbosynth), 2 mM, polyamine uptake inhibitor
382 AMXT 1501 (Aminex Therapeutics), 1 μM was used for polyamine mixture, unless specifically
383 indicated, a 3 μM polyamine mixture (putrescine 1μM, spermidine 1μM, spermine 1μM) was used
384 for cell culture. In order to prevent diamine oxidase in the FBS from breaking down the polyamine
385 supplement in cell culture, 0.2 mM aminoguanidine (Sigma) was added to all polyamine
386 supplemented groups.

387 **Cell cycle analysis**

388 Upon *in vitro* activation, T cell cycle analysis was performed using Phase-Flow Alexa Fluro 647
389 BrdU Kit (Biolegend) per the manufacturer's instructions. Briefly, T cells were pulsed with 10
390 μg/mL BrdU for 1 hour before being processed with surface staining, fixation, and
391 permeabilization. BrdU incorporated into the DNA during S phase were recognized by intracellular

392 BrdU antibody staining, and total DNA content was used to differentiate G1 and G2 stages by
393 7AAD labeling.

394 **qPCR**

395 Total RNA was isolated using the RNeasy Mini Kit (Qiagen) and was reverse transcribed using
396 random hexamers and M-MLV Reverse Transcriptase (Invitrogen). SYBR green-based quantitative
397 RT-PCR was performed using the Applied Biosystems 7900 Real Time PCR System. The relative
398 gene expression was determined by the comparative C_T method, also referred to as the $2^{-\Delta\Delta C_T}$
399 method. The data were presented as the fold change in gene expression normalized to an internal
400 reference gene (beta2-microglobulin) and relative to the control (the first sample in the group). Fold
401 change=$2^{-\Delta\Delta C_T}$=[($C_{T\text{gene of interst}}$- $C_{T\text{internal reference}}$)]sample A-[($C_{T\text{gene of interst}}$- $C_{T\text{internal reference}}$)]sample
402 B. Samples for each experimental condition were run in triplicated PCR reactions. Primer
403 sequences were obtained from Primer Bank.

404 **Putrescine uptake assay**

405 2X10^6 T cells were suspended in 200ul PBS containing permeant putrescine (100 μM) and [1,4-
406 ^{14}C]-putrescine dihydrochloride (0.2 uCi, ARC 0245) and incubated at 37°C for 10 minutes (within
407 the established linear phase of uptake). The reaction was stopped by loading all the transport
408 mixture onto a discontinuous gradient of bromododecane and perchloric acid/sucrose and then
409 centrifuged at 14, 000 ×*g* for 90 seconds. The discontinuous gradient was prepared by overlaying
410 1-Bromododecane (800 μL; Sigma-Aldrich) above 100 μL of 20% perchloric acid (Sigma-
411 Aldrich)/8% sucrose solution in 1.5-ml microfuge tube. The samples were snap-frozen in an
412 ethanol-dry ice bath. The bottom part of microfuge tubes containing T cell lysate in perchloric acid-
413 sucrose was cut by a microfuge cutter, washed with 300 μL of 0.5%SDS-1%TritonX100, and
414 transferred into scintillation vials. 10 mL scintillation cocktail was then added to each vial, and the
415 radioactivity was then quantitated by liquid scintillation spectrometry.

416 **Adoptive cell transfer and *in vivo* proliferation**

417 For homeostatic proliferation in lymphopenic *Rag*$^{-/-}$ mice, naïve CD4+ T cells isolated from donor
418 mice using naïve CD4+ mouse T cell isolation kit (Biolegend) were labeled with CFSE.
419 Approximately 1x10^{7} cells in 150 μL PBS were transferred via retro-orbital venous injection into
420 6-8 week-old gender-matched host mice. Mice were sacrificed after 4 days and lymph nodes were
421 extracted from host mice, then processed for surface staining and flow analysis.

422 For antigen driven proliferation using OTII mice: naïve CD4+ T cells isolated from OTII/CD45.2
423 TCR transgenic donor mice using naïve CD4+ mouse T cell isolation kit (Biolegend) were labeled
424 with CFSE. Approximately 1x10^{7} cells in 150 μL PBS were transferred via retro-orbital venous
425 injection into 6-8 week-old gender-matched WT/CD45.1 host mice. Host mice were immunized
426 subcutaneously in the hock area (50 μL each site) in both legs with 1 mg/mL OVA$^{323-339}$ peptide
427 (InvivoGen) emulsified with CFA (InvivoGen). After 7 days of antigen-driven proliferation, lymph
428 organs were extracted from host mice then processed for surface staining and flow analysis.

429 **Experimental Autoimmune Encephalomyelitis (EAE)**

430 For induced EAE, mice were immunized subcutaneously with 100 μg of myelin oligodendrocyte
431 glycoprotein (MOG)$_{35–55}$ peptide emulsified in complete freund adjuvant (CFA), which was made
432 from IFA(Difco) plus mycobacterium tuberculosis (Difco). Mice were i.p. injected with 200 ng of
433 pertussis toxin (List Biological,#181) on the day of immunization and 2 days later. For the DFMO
434 (Carbosynth) treated group, mice were fed with 1% DFMO in drinking water throughout the
435 experiment. DFMO water was replenished every five days. For the AMXT 1501 (Aminex
436 Therapeutics) treated group, mice received 3mg/kg of AMXT 1501 subcutaneous daily throughout
437 the experiment. The mice were observed daily for clinical signs and scored as described below.

Score 1	Limp tail. When the mouse is picked up by the tail, the whole tail drapes over your finger, instead of being erect.
Score 2	Limp tail and weakness of hind legs. When mouse is picked up by tail, legs are not spread apart, but held closer together. When the mouse is observed when walking, it has a clearly apparent wobbly walk.
Score 3	Limp tail and complete paralysis of hind legs (most common). OR Limp tail with paralysis of one front and one hind legs.
Score 4	Limp tail, complete hind leg and partial front leg paralysis. Mouse is minimally moving around the cage but appears alert and feeding. Usually, euthanasia is recommended

438

439 **CE-QqQ/TOFMS analysis**

440

441 Total mouse T cells with 75-80% CD3 positivity were isolated from WT or ODC cKO mice.
442 Isolated cells were activated with plate-bound anti-CD3 (2 μg/mL) and anti-CD28 (2 μg/mL)
443 antibodies with IL-2 (5 ng/mL), and were cultured in 6-well plates for 36 hours. Activated cells
444 (around 1.5×10^7 cells/sample) was used for the extraction of intracellular metabolites. The cells
445 were collected by centrifugation (300 ×*g* at 4ºC for 5 min) and washed twice with 5% mannitol
446 solution (10 mL first and then 2 mL). The cells were then treated with 800 μL of methanol and
447 vortexed for 30 s in order to inactivate enzymes. Next, the cell extract was treated with 550 μL of
448 Milli-Q water containing internal standards (H3304-1002, Human Metabolome Technologies, inc.,
449 Tsuruoka, Japan) and vortexed for 30 s. The extract was obtained and centrifuged at 2,300 ×*g* and
450 4ºC for 5 min, and then 700 μL of upper aqueous layer was centrifugally filtered through a Millipore
451 5-kDa cutoff filter at 9,100 ×*g* and 4ºC for 180 min to remove proteins. The filtrate was centrifugally
452 concentrated and re-suspended in 50 μL of Milli-Q water for CE-MS analysis.

453 Cationic compounds were measured in the positive mode of CE-TOFMS and anionic compounds
454 were measured in the positive and negative modes of CE-MS/MS according to the methods
455 developed by Soga, *et al* [PMID:10740865, PMID:12038746, PMID:14582645].
456 Peaks detected by CE-TOFMS and CE-MS/MS were extracted using an automatic integration
457 software (MasterHands, Keio University, Tsuruoka, Japan [PMID: 20300169] and MassHunter
458 Quantitative Analysis B.04.00, Agilent Technologies, Santa Clara, CA, USA, respectively) in order
459 to obtain peak information including *m/z*, migration time (MT), and peak area. The peaks were
460 annotated with putative metabolites from the HMT metabolite database based on their MTs in CE
461 and *m*/*z* values determined by TOFMS. The tolerance range for the peak annotation was configured
462 at ±0.5 min for MT and ±10 ppm for *m/z*. In addition, concentrations of metabolites were calculated
463 by normalizing the peak area of each metabolite with respect to the area of the internal standard
464 and by using standard curves, which were obtained by three-point calibrations.
465 Hierarchical cluster analysis (HCA) and principal component analysis (PCA) were performed by
466 our proprietary software, PeakStat and SampleStat, respectively.
467 Detected metabolites were plotted on metabolic pathway maps using VANTED (Visualization and
468 Analysis of Networks containing Experimental Data) software [PMID:16519817].
469
470
471 **CE-TOFMS analysis**
472
473 Total mouse T cells were isolated from spleen and lymph nodes of WT mice and were activated in
474 6-well plates by plate-bound anti-CD3 (2 μg/mL) and anti-CD28 (2 μg/mL) antibodies with IL-2
475 (5 ng/mL) in conditional media (Gln, Arg, Pro triple-free RPMI-1640 medium) containing 2 mM
476 $^{13}C_5$-Glutamine, 1.15 mM $^{13}C_6$-Arginine, or 0.17 mM $^{13}C_5$-Proline, respectively, for 36 hours.
477 Activated cells (around 1.8×10^7 cells/sample) was used for the extraction of intracellular

478 metabolites. The cells were collected by centrifugation (300 ×*g* at 4ºC for 5 min) and washed twice
479 with 5% mannitol solution (10 mL first and then 2 mL). The cells were then treated with 800 µL of
480 methanol and vortexed for 30 s in order to inactivate enzymes. Next, the cell extract was treated
481 with 550 µL of Milli-Q water containing internal standards (H3304-1002, Human Metabolome
482 Technologies, Inc., Tsuruoka, Japan) and vortexed for 30 s. The extract was obtained and
483 centrifuged at 2,300 ×*g* and 4ºC for 5 min, and then 700 µL of upper aqueous layer was centrifugally
484 filtered through a Millipore 5-kDa cutoff filter at 9,100 ×*g* and 4ºC for 180 min to remove proteins.
485 The filtrate was centrifugally concentrated and re-suspended in 50 µL of Milli-Q water for CE-MS
486 analysis. Metabolome measurements were carried out through a facility service at Human
487 Metabolome Technology Inc., Tsuruoka, Japan. Hierarchical cluster analysis (HCA) and principal
488 component analysis (PCA) were performed by our proprietary software, PeakStat and SampleStat,
489 respectively. Detected metabolites were plotted on metabolic pathway maps using VANTED
490 (Visualization and Analysis of Networks containing Experimental Data) software.
491
492 CE-TOFMS measurement was carried out using an Agilent CE Capillary Electrophoresis System
493 equipped with an Agilent 6210 Time of Flight mass spectrometer, Agilent 1100 isocratic HPLC
494 pump, Agilent G1603A CE-MS adapter kit, and Agilent G1607A CE-ESI-MS sprayer kit (Agilent
495 Technologies, Waldbronn, Germany). The systems were controlled by Agilent G2201AA
496 ChemStation software version B.03.01 for CE (Agilent Technologies, Waldbronn, Germany). The
497 metabolites were analyzed by using a fused silica capillary (50 µm *i.d.* × 80 cm total length), with
498 commercial electrophoresis buffer (Solution ID: H3301-1001 for cation analysis and H3302-1021
499 for anion analysis, Human Metabolome Technologies) as the electrolyte. The sample was injected
500 at a pressure of 50 mbar for 10 s (approximately 10 nL) in cation analysis and 25 s (approximately
501 25 nL) in anion analysis. The spectrometer was scanned from *m/z* 50 to 1,000. Other conditions
502 were as described previously [PMID:10740865, PMID:12038746, PMID:14582645].

503

504 **Statistical analysis**

505 Statistical analysis was conducted using the GraphPad Prism software (GraphPad Software, Inc.).
506 P values were calculated with two-way ANOVA for the EAE experiments. Unpaired two tail
507 student's t-test was used to assess differences in all other experiments. P values smaller than 0.05
508 were considered significant, with p-values<0.05, p-values<0.01, and p-values<0.001 indicated as
509 *, **, and ***, respectively.

510 **References**

511

512 1. D. Finlay, D. A. Cantrell, Metabolism, migration and memory in cytotoxic T cells. *Nature*
513 *reviews. Immunology* **11**, 109-117 (2011).
514 2. R. Wang, D. R. Green, Metabolic checkpoints in activated T cells. *Nat Immunol* **13**, 907-
515 915 (2012).
516 3. M. Slack, T. Wang, R. Wang, T cell metabolic reprogramming and plasticity. *Molecular*
517 *immunology* **68**, 507-512 (2015).
518 4. S. E. Weinberg, L. A. Sena, N. S. Chandel, Mitochondria in the regulation of innate and
519 adaptive immunity. *Immunity* **42**, 406-417 (2015).
520 5. L. A. O'Neill, R. J. Kishton, J. Rathmell, A guide to immunometabolism for
521 immunologists. *Nature reviews. Immunology* **16**, 553-565 (2016).
522 6. C. H. Patel, J. D. Powell, Targeting T cell metabolism to regulate T cell activation,
523 differentiation and function in disease. *Current opinion in immunology* **46**, 82-88 (2017).
524 7. H. Zeng, H. Chi, mTOR signaling in the differentiation and function of regulatory and
525 effector T cells. *Current opinion in immunology* **46**, 103-111 (2017).

526 8. F. Blachier, M. Selamnia, V. Robert, H. M'Rabet-Touil, P. H. Duee, Metabolism of L-
527 arginine through polyamine and nitric oxide synthase pathways in proliferative or
528 differentiated human colon carcinoma cells. *Biochim Biophys Acta* **1268**, 255-262 (1995).
529 9. K. Saitoh *et al.*, Role of thoracotomy in pulmonary metastases from gestational
530 choriocarcinoma. *J Thorac Cardiovasc Surg* **85**, 815-820 (1983).
531 10. T. Maeda *et al.*, Role of polyamines derived from arginine in differentiation and
532 proliferation of human blood cells. *Biol Pharm Bull* **29**, 234-239 (2006).
533 11. R. F. Bertolo, D. G. Burrin, Comparative aspects of tissue glutamine and proline
534 metabolism. *J Nutr* **138**, 2032S-2039S (2008).
535 12. G. Wu, A. G. Borbolla, D. A. Knabe, The uptake of glutamine and release of arginine,
536 citrulline and proline by the small intestine of developing pigs. *J Nutr* **124**, 2437-2444
537 (1994).
538 13. R. Majumdar *et al.*, Glutamate, Ornithine, Arginine, Proline, and Polyamine Metabolic
539 Interactions: The Pathway Is Regulated at the Post-Transcriptional Level. *Front Plant Sci*
540 **7**, 78 (2016).
541 14. N. C. Munoz-Esparza *et al.*, Polyamines in Food. *Front Nutr* **6**, 108 (2019).
542 15. B. Ramos-Molina, M. I. Queipo-Ortuno, A. Lambertos, F. J. Tinahones, R. Penafiel,
543 Dietary and Gut Microbiota Polyamines in Obesity- and Age-Related Diseases. *Front*
544 *Nutr* **6**, 24 (2019).
545 16. A. E. Pegg, Functions of Polyamines in Mammals. *J Biol Chem* **291**, 14904-14912 (2016).
546 17. K. Igarashi, K. Kashiwagi, Modulation of cellular function by polyamines. *Int J Biochem*
547 *Cell Biol* **42**, 39-51 (2010).
548 18. L. Miller-Fleming, V. Olin-Sandoval, K. Campbell, M. Ralser, Remaining Mysteries of
549 Molecular Biology: The Role of Polyamines in the Cell. *J Mol Biol* **427**, 3389-3406
550 (2015).

551 19. D. Teti, M. Visalli, H. McNair, Analysis of polyamines as markers of (patho)physiological
552 conditions. *J Chromatogr B Analyt Technol Biomed Life Sci* **781**, 107-149 (2002).
553 20. E. Karouzakis, R. E. Gay, S. Gay, M. Neidhart, Increased recycling of polyamines is
554 associated with global DNA hypomethylation in rheumatoid arthritis synovial fibroblasts.
555 *Arthritis Rheum* **64**, 1809-1817 (2012).
556 21. L. Xu *et al.*, Arginase and autoimmune inflammation in the central nervous system.
557 *Immunology* **110**, 141-148 (2003).
558 22. V. Bronte, P. Zanovello, Regulation of immune responses by L-arginine metabolism.
559 *Nature reviews. Immunology* **5**, 641-654 (2005).
560 23. A. Yurdagul, Jr. *et al.*, Macrophage Metabolism of Apoptotic Cell-Derived Arginine
561 Promotes Continual Efferocytosis and Resolution of Injury. *Cell Metab* **31**, 518-533 e510
562 (2020).
563 24. R. Wang *et al.*, The transcription factor Myc controls metabolic reprogramming upon T
564 lymphocyte activation. *Immunity* **35**, 871-882 (2011).
565 25. R. Geiger *et al.*, L-Arginine Modulates T Cell Metabolism and Enhances Survival and
566 Anti-tumor Activity. *Cell* **167**, 829-842 e813 (2016).
567 26. D. J. Puleston *et al.*, Polyamines and eIF5A Hypusination Modulate Mitochondrial
568 Respiration and Macrophage Activation. *Cell Metab* **30**, 352-363 e358 (2019).
569 27. D. M. Hardbower *et al.*, Ornithine decarboxylase regulates M1 macrophage activation and
570 mucosal inflammation via histone modifications. *Proc Natl Acad Sci U S A* **114**, E751-
571 E760 (2017).
572 28. H. Zhang *et al.*, Polyamines Control eIF5A Hypusination, TFEB Translation, and
573 Autophagy to Reverse B Cell Senescence. *Mol Cell* **76**, 110-125 e119 (2019).
574 29. P. J. Murray, Amino acid auxotrophy as a system of immunological control nodes. *Nat*
575 *Immunol* **17**, 132-139 (2016).

576 30. L. A. Van de Velde *et al.*, T Cells Encountering Myeloid Cells Programmed for Amino
577 Acid-dependent Immunosuppression Use Rictor/mTORC2 Protein for Proliferative
578 Checkpoint Decisions. *J Biol Chem* **292**, 15-30 (2017).
579 31. C. Liu, N. M. Chapman, P. W. Karmaus, H. Zeng, H. Chi, mTOR and metabolic
580 regulation of conventional and regulatory T cells. *J Leukoc Biol* **97**, 837-847 (2015).
581 32. J. Blagih *et al.*, The energy sensor AMPK regulates T cell metabolic adaptation and
582 effector responses in vivo. *Immunity* **42**, 41-54 (2015).
583 33. J. N. R. Gnanaprakasam, J. W. Sherman, R. Wang, MYC and HIF in shaping immune
584 response and immune metabolism. *Cytokine Growth Factor Rev* **35**, 63-70 (2017).
585 34. Y. Kidani, S. J. Bensinger, Liver X receptor and peroxisome proliferator-activated
586 receptor as integrators of lipid homeostasis and immunity. *Immunological reviews* **249**,
587 72-83 (2012).
588 35. R. J. Kishton *et al.*, AMPK Is Essential to Balance Glycolysis and Mitochondrial
589 Metabolism to Control T-ALL Cell Stress and Survival. *Cell Metab* **23**, 649-662 (2016).
590 36. I. H. Sun *et al.*, mTOR Complex 1 Signaling Regulates the Generation and Function of
591 Central and Effector Foxp3(+) Regulatory T Cells. *J Immunol* **201**, 481-492 (2018).
592 37. E. H. Ma *et al.*, Metabolic Profiling Using Stable Isotope Tracing Reveals Distinct
593 Patterns of Glucose Utilization by Physiologically Activated CD8(+) T Cells. *Immunity*
594 **51**, 856-870 e855 (2019).
595 38. R. Wang, D. R. Green, Metabolic reprogramming and metabolic dependency in T cells.
596 *Immunological reviews* **249**, 14-26 (2012).
597 39. H. Pendeville *et al.*, The ornithine decarboxylase gene is essential for cell survival during
598 early murine development. *Mol Cell Biol* **21**, 6549-6558 (2001).
599 40. W. C. Skarnes *et al.*, A conditional knockout resource for the genome-wide study of
600 mouse gene function. *Nature* **474**, 337-342 (2011).

601 41. E. Larque, M. Sabater-Molina, S. Zamora, Biological significance of dietary polyamines.
602 *Nutrition* **23**, 87-95 (2007).
603 42. M. R. Burns, G. F. Graminski, R. S. Weeks, Y. Chen, T. G. O'Brien, Lipophilic lysine-
604 spermine conjugates are potent polyamine transport inhibitors for use in combination with
605 a polyamine biosynthesis inhibitor. *J Med Chem* **52**, 1983-1993 (2009).
606 43. K. Samal *et al.*, AMXT-1501, a novel polyamine transport inhibitor, synergizes with
607 DFMO in inhibiting neuroblastoma cell proliferation by targeting both ornithine
608 decarboxylase and polyamine transport. *Int J Cancer* **133**, 1323-1333 (2013).
609 44. S. B. Gitto *et al.*, Difluoromethylornithine Combined with a Polyamine Transport
610 Inhibitor Is Effective against Gemcitabine Resistant Pancreatic Cancer. *Mol Pharm* **15**,
611 369-376 (2018).
612 45. L. D. Gamble *et al.*, Inhibition of polyamine synthesis and uptake reduces tumor
613 progression and prolongs survival in mouse models of neuroblastoma. *Sci Transl Med* **11**,
614 (2019).
615 46. P. G. Kennedy, Clinical features, diagnosis, and treatment of human African
616 trypanosomiasis (sleeping sickness). *Lancet Neurol* **12**, 186-194 (2013).
617 47. A. C. Vissing, E. H. Taudorf, C. S. Haak, P. A. Philipsen, M. Haedersdal, Adjuvant
618 eflornithine to maintain IPL-induced hair reduction in women with facial hirsutism: a
619 randomized controlled trial. *J Eur Acad Dermatol Venereol* **30**, 314-319 (2016).
620 48. N. LoGiudice, L. Le, I. Abuan, Y. Leizorek, S. C. Roberts, Alpha-
621 Difluoromethylornithine, an Irreversible Inhibitor of Polyamine Biosynthesis, as a
622 Therapeutic Strategy against Hyperproliferative and Infectious Diseases. *Med Sci (Basel)*
623 **6**, (2018).
624 49. R. R. Somani, P. R. Rai, P. S. Kandpile, Ornithine Decarboxylase Inhibition: A Strategy to
625 Combat Various Diseases. *Mini Rev Med Chem* **18**, 1008-1021 (2018).

626 50. R. A. Casero, Jr., T. Murray Stewart, A. E. Pegg, Polyamine metabolism and cancer:
627 treatments, challenges and opportunities. *Nat Rev Cancer* **18**, 681-695 (2018).
628 51. S. L. Nowotarski, P. M. Woster, R. A. Casero, Jr., Polyamines and cancer: implications
629 for chemotherapy and chemoprevention. *Expert Rev Mol Med* **15**, e3 (2013).
630 52. G. Wu, F. W. Bazer, J. Hu, G. A. Johnson, T. E. Spencer, Polyamine synthesis from
631 proline in the developing porcine placenta. *Biol Reprod* **72**, 842-850 (2005).
632 53. P. C. Rodriguez, A. C. Ochoa, A. A. Al-Khami, Arginine Metabolism in Myeloid Cells
633 Shapes Innate and Adaptive Immunity. *Frontiers in immunology* **8**, 93 (2017).
634 54. A. Werner *et al.*, Reconstitution of T Cell Proliferation under Arginine Limitation:
635 Activated Human T Cells Take Up Citrulline via L-Type Amino Acid Transporter 1 and
636 Use It to Regenerate Arginine after Induction of Argininosuccinate Synthase Expression.
637 *Frontiers in immunology* **8**, 864 (2017).
638 55. S. Weis *et al.*, Metabolic Adaptation Establishes Disease Tolerance to Sepsis. *Cell* **169**,
639 1263-1275 e1214 (2017).
640 56. E. D. Weinberg, Nutritional immunity. Host's attempt to withold iron from microbial
641 invaders. *JAMA* **231**, 39-41 (1975).
642 57. Y. Abu Kwaik, D. Bumann, Microbial quest for food in vivo: 'nutritional virulence' as an
643 emerging paradigm. *Cell Microbiol* **15**, 882-890 (2013).
644 58. K. Troha, J. S. Ayres, Metabolic Adaptations to Infections at the Organismal Level.
645 *Trends Immunol* **41**, 113-125 (2020).
646 59. S. J. Bensinger *et al.*, LXR signaling couples sterol metabolism to proliferation in the
647 acquired immune response. *Cell* **134**, 97-111 (2008).
648 60. V. A. Gerriets, J. C. Rathmell, Metabolic pathways in T cell fate and function. *Trends in*
649 *immunology* **33**, 168-173 (2012).

650 61. E. L. Pearce, M. C. Poffenberger, C. H. Chang, R. G. Jones, Fueling immunity: insights
651 into metabolism and lymphocyte function. *Science* **342**, 1242454 (2013).
652 62. H. Chi, Regulation and function of mTOR signalling in T cell fate decisions. *Nature*
653 *Reviews Immunology* **12**, 325-338 (2012).
654 63. J. D. Powell, G. M. Delgoffe, The mammalian target of rapamycin: linking T cell
655 differentiation, function, and metabolism. *Immunity* **33**, 301-311 (2010).
656 64. R. D. Michalek, J. C. Rathmell, The metabolic life and times of a T-cell. *Immunological*
657 *reviews* **236**, 190-202 (2010).
658 65. P. C. Ho *et al.*, Phosphoenolpyruvate Is a Metabolic Checkpoint of Anti-tumor T Cell
659 Responses. *Cell* **162**, 1217-1228 (2015).
660 66. M. R. Sullivan *et al.*, Quantification of microenvironmental metabolites in murine cancers
661 reveals determinants of tumor nutrient availability. *Elife* **8**, (2019).
662 67. J. R. Cantor *et al.*, Physiologic Medium Rewires Cellular Metabolism and Reveals Uric
663 Acid as an Endogenous Inhibitor of UMP Synthase. *Cell* **169**, 258-272 e217 (2017).
664 68. A. Muir *et al.*, Environmental cystine drives glutamine anaplerosis and sensitizes cancer
665 cells to glutaminase inhibition. *Elife* **6**, (2017).
666 69. Z. T. Schug *et al.*, Acetyl-CoA synthetase 2 promotes acetate utilization and maintains
667 cancer cell growth under metabolic stress. *Cancer Cell* **27**, 57-71 (2015).
668 70. J. R. Cantor, The Rise of Physiologic Media. *Trends Cell Biol* **29**, 854-861 (2019).
669 71. T. Ackermann, S. Tardito, Cell Culture Medium Formulation and Its Implications in
670 Cancer Metabolism. *Trends Cancer* **5**, 329-332 (2019).
671 72. E. Kvamme, G. Svenneby, Effect of anaerobiosis and addition of keto acids on glutamine
672 utilization by Ehrlich ascites-tumor cells. *Biochim Biophys Acta* **42**, 187-188 (1960).
673 73. R. J. DeBerardinis, J. J. Lum, G. Hatzivassiliou, C. B. Thompson, The biology of cancer:
674 metabolic reprogramming fuels cell growth and proliferation. *Cell Metab* **7**, 11-20 (2008).

675 74. B. J. Altman, Z. E. Stine, C. V. Dang, From Krebs to clinic: glutamine metabolism to
676 cancer therapy. *Nat Rev Cancer* **16**, 619-634 (2016).
677 75. S. M. Morris, Jr., Arginine metabolism: boundaries of our knowledge. *J Nutr* **137**, 1602S-
678 1609S (2007).
679 76. E. L. Carr *et al.*, Glutamine uptake and metabolism are coordinately regulated by
680 ERK/MAPK during T lymphocyte activation. *J Immunol* **185**, 1037-1044 (2011).
681 77. G. Lian *et al.*, Glutathione de novo synthesis but not recycling process coordinates with
682 glutamine catabolism to control redox homeostasis and directs murine T cell
683 differentiation. *Elife* **7**, (2018).
684 78. M. O. Johnson *et al.*, Distinct Regulation of Th17 and Th1 Cell Differentiation by
685 Glutaminase-Dependent Metabolism. *Cell* **175**, 1780-1795 e1719 (2018).
686 79. D. Klysz *et al.*, Glutamine-dependent alpha-ketoglutarate production regulates the balance
687 between T helper 1 cell and regulatory T cell generation. *Sci Signal* **8**, ra97 (2015).
688 80. S. M. Lange *et al.*, l-Citrulline Metabolism in Mice Augments CD4(+) T Cell Proliferation
689 and Cytokine Production In Vitro, and Accumulation in the Mycobacteria-Infected Lung.
690 *Frontiers in immunology* **8**, 1561 (2017).
691 81. J. L. Deignan *et al.*, Polyamine homeostasis in arginase knockout mice. *Am J Physiol Cell*
692 *Physiol* **293**, C1296-1301 (2007).
693 82. J. L. Deignan *et al.*, Ornithine deficiency in the arginase double knockout mouse. *Mol*
694 *Genet Metab* **89**, 87-96 (2006).
695 83. C. V. Dang, MYC, metabolism, cell growth, and tumorigenesis. *Cold Spring Harbor*
696 *perspectives in medicine* **3**, (2013).
697 84. T. Wang, G. Liu, R. Wang, The Intercellular Metabolic Interplay between Tumor and
698 Immune Cells. *Frontiers in immunology* **5**, 358 (2014).

699 85. N. N. Pavlova, C. B. Thompson, The Emerging Hallmarks of Cancer Metabolism. *Cell*
700 *Metab* **23**, 27-47 (2016).
701 86. D. O'Sullivan, E. L. Pearce, Targeting T cell metabolism for therapy. *Trends Immunol* **36**,
702 71-80 (2015).
703 87. R. A. Cairns, I. S. Harris, T. W. Mak, Regulation of cancer cell metabolism. *Nat Rev*
704 *Cancer* **11**, 85-95 (2011).
705 88. P. P. Hsu, D. M. Sabatini, Cancer cell metabolism: Warburg and beyond. *Cell* **134**, 703-
706 707 (2008).
707 89. L. Antonioli, C. Blandizzi, P. Pacher, G. Hasko, Immunity, inflammation and cancer: a
708 leading role for adenosine. *Nat Rev Cancer* **13**, 842-857 (2013).
709 90. X. Xu, J. N. R. Gnanaprakasam, J. Sherman, R. Wang, A Metabolism Toolbox for CAR T
710 Therapy. *Front Oncol* **9**, 322 (2019).
711 91. A. Arruabarrena-Aristorena, A. Zabala-Letona, A. Carracedo, Oil for the cancer engine:
712 The cross-talk between oncogenic signaling and polyamine metabolism. *Sci Adv* **4**,
713 eaar2606 (2018).
714 92. E. W. Gerner, F. L. Meyskens, Jr., Polyamines and cancer: old molecules, new
715 understanding. *Nat Rev Cancer* **4**, 781-792 (2004).
716 93. C. Bello-Fernandez, G. Packham, J. L. Cleveland, The ornithine decarboxylase gene is a
717 transcriptional target of c-Myc. *Proc Natl Acad Sci U S A* **90**, 7804-7808 (1993).
718 94. R. J. Rounbehler *et al.*, Targeting ornithine decarboxylase impairs development of
719 MYCN-amplified neuroblastoma. *Cancer Res* **69**, 547-553 (2009).
720 95. A. A. Abdulhussein, H. M. Wallace, Polyamines and membrane transporters. *Amino Acids*
721 **46**, 655-660 (2014).

722 96. T. Uemura, D. E. Stringer, K. A. Blohm-Mangone, E. W. Gerner, Polyamine transport is
723 mediated by both endocytic and solute carrier transport mechanisms in the gastrointestinal
724 tract. *Am J Physiol Gastrointest Liver Physiol* **299**, G517-522 (2010).
725 97. M. Hiasa *et al.*, Identification of a mammalian vesicular polyamine transporter. *Sci Rep* **4**,
726 6836 (2014).
727 98. S. van Veen *et al.*, ATP13A2 deficiency disrupts lysosomal polyamine export. *Nature*
728 **578**, 419-424 (2020).
729 99. J. L. Mitchell, T. K. Thane, J. M. Sequeira, R. Thokala, Unusual aspects of the polyamine
730 transport system affect the design of strategies for use of polyamine analogues in
731 chemotherapy. *Biochem Soc Trans* **35**, 318-321 (2007).

732 **Acknowledgments**

733

734 Acknowledgments, when needed, should include the following information in the order
735 listed below, a single paragraph, starting with the word "**Acknowledgments:**" in bold.
736 Please use the subhead and boldface layout as shown below.).
737 **General**: We thank John Sherman and Hayley Rodgers for critically reading and editing the
738 manuscript.
739 **Funding:** This work was supported by 1R21CA227926-01A1 and 1UO1CA232488-01 from
740 National Institute of Health (Cancer Moonshot program), 1R01AI114581 from National
741 Institute of Health, V2014-001 from the V-Foundation and 128436-RSG-15-180-01-LIB
742 from the American Cancer Society (to RW).
743 **Competing interests:** M.R.B. currently is the president and CSO of Aminex Therapeutics Inc,
744 which is a pharmaceutical start-up company that actively develops polyamine blocking
745 agents. All other authors declare no conflict of interest.

746

747 **Figures**

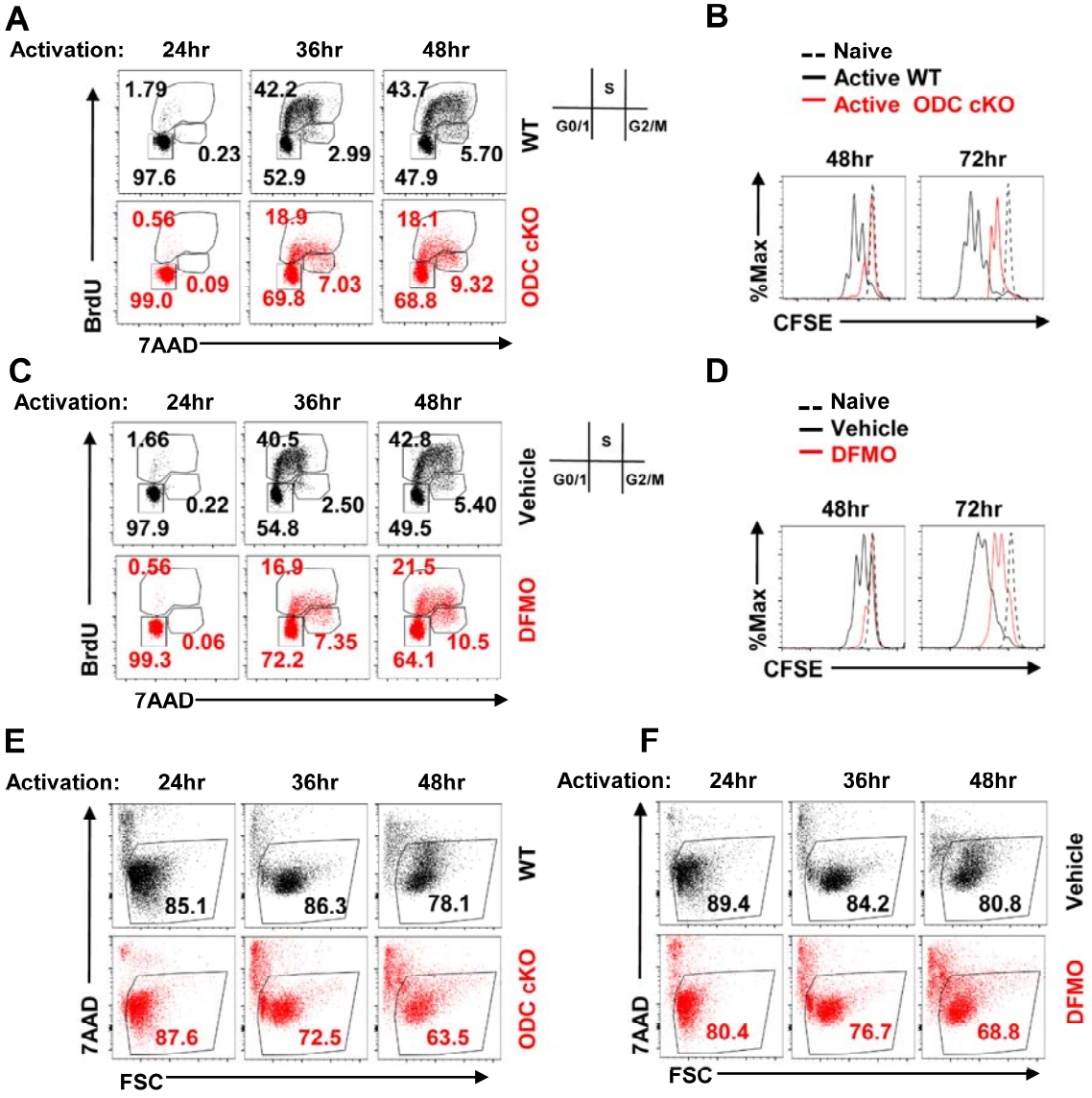

Figure 1. Blockage of de novo polyamine biosynthesis suppresses T cell proliferation and reduces viability in vitro.

748

749

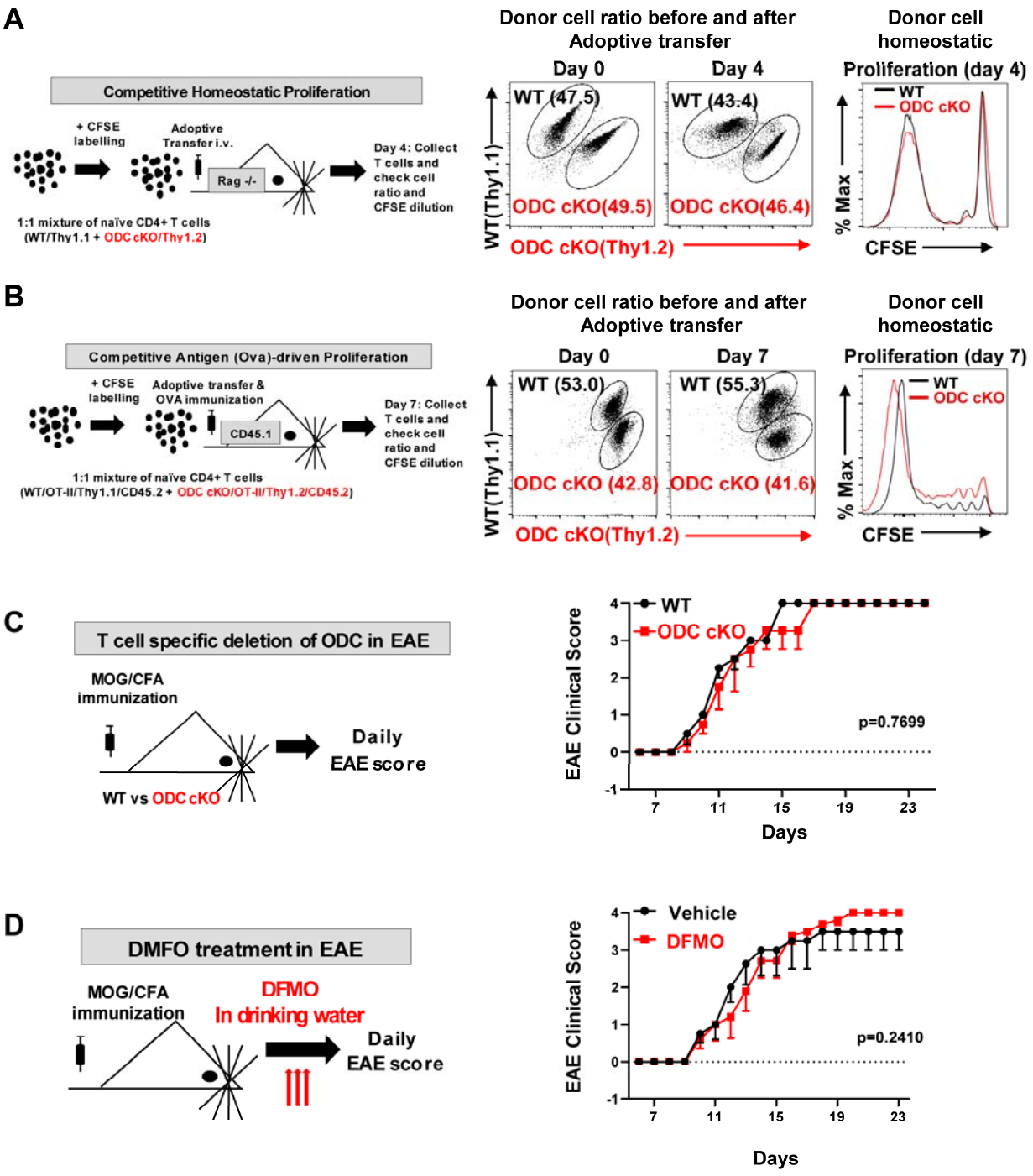

Figure 2. De novo polyamine biosynthesis is dispensable for driving T cell proliferation and function in vivo.

750

751

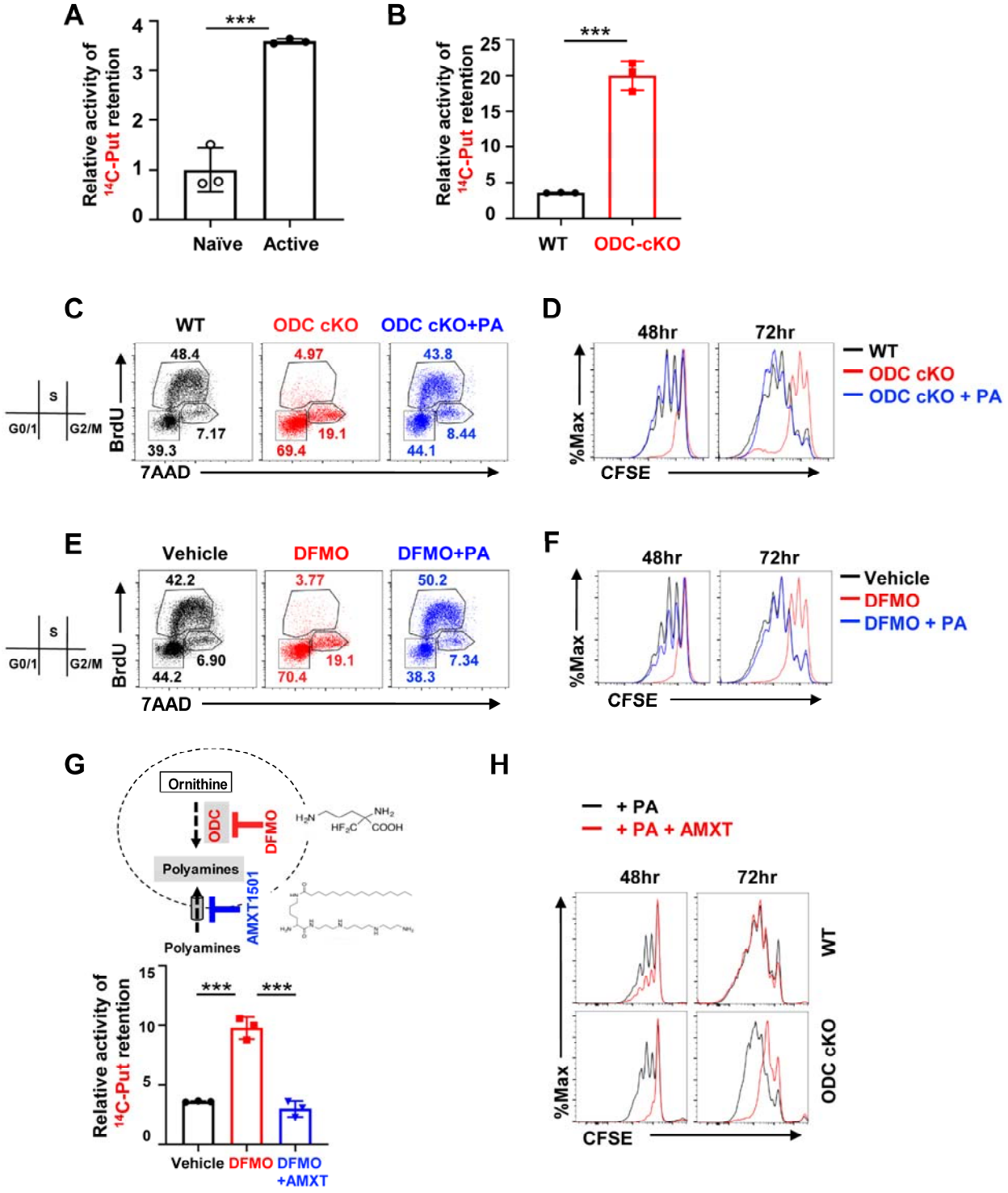

Figure 3. Ablation of de novo polyamine biosynthesis renders T cell dependent on polyamine uptake that can be blocked by AMXT1501.

752

753

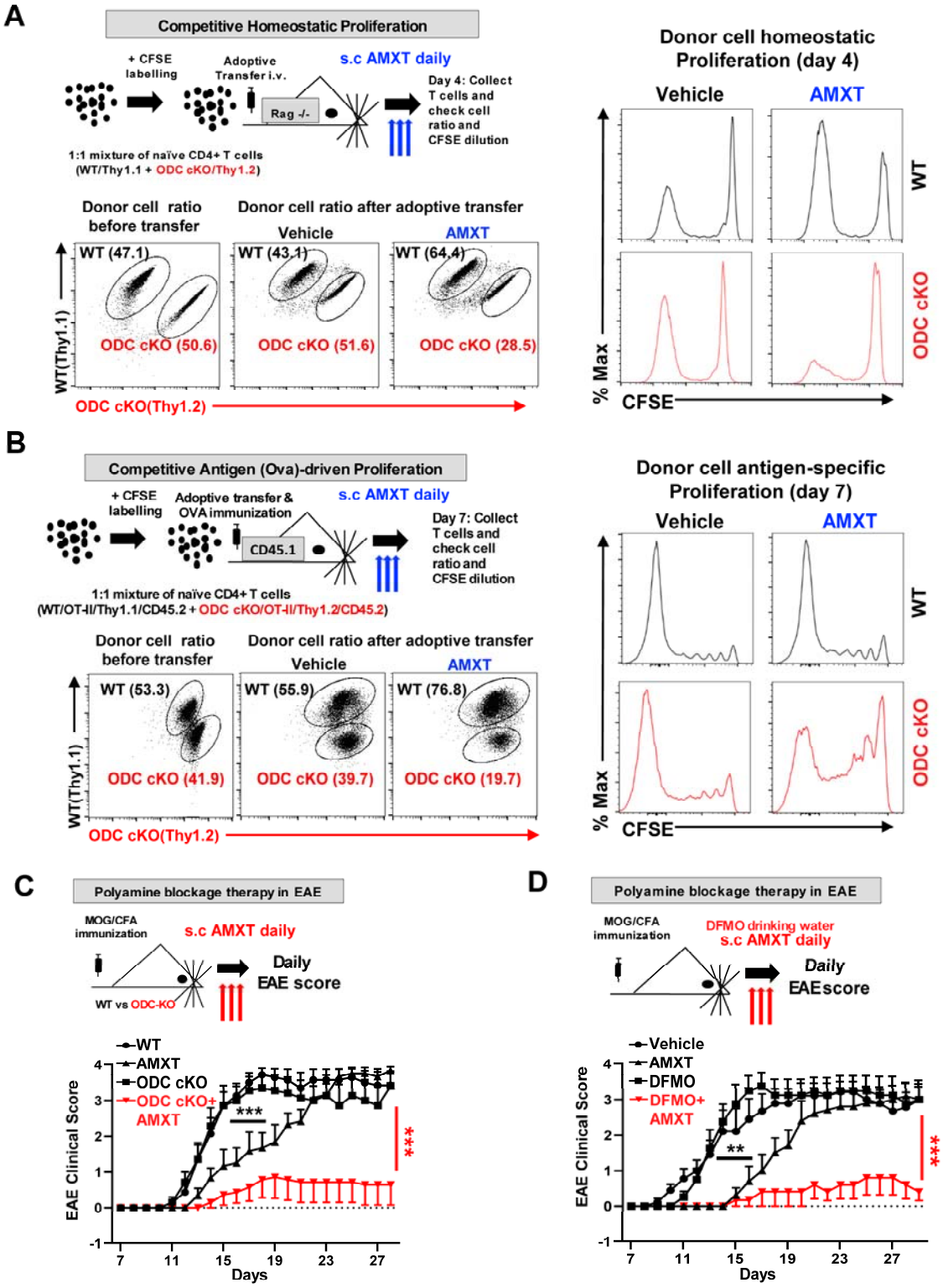

Figure 4. Simultaneous blockage of polyamine uptake and de novo biosynthesis suppresses T cell proliferation and function in vivo.

754

755

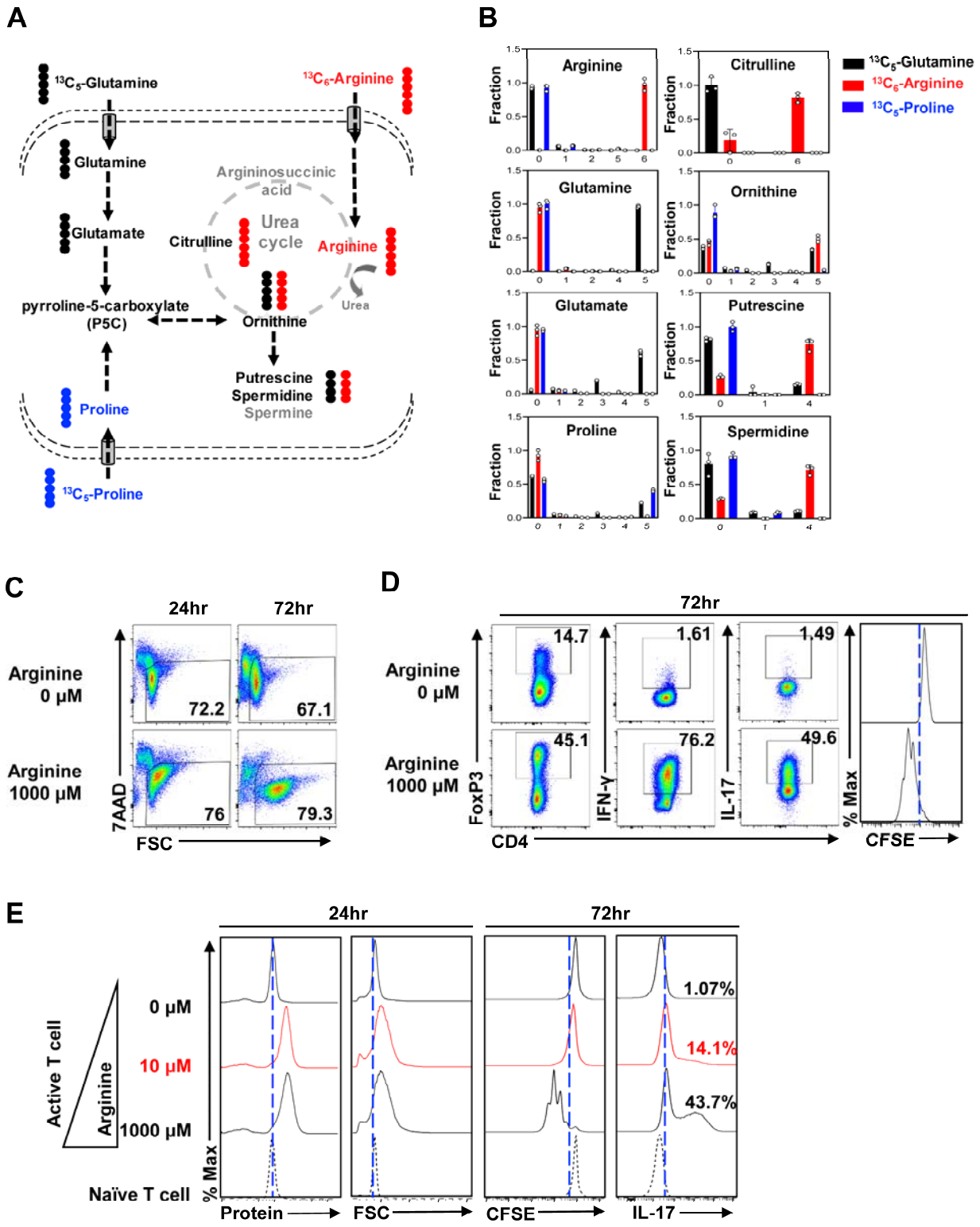

Figure 5. Arginine catabolism supports polyamine biosynthesis and T cell proliferation.

758 **Figure 1. Blockage of de novo polyamine biosynthesis suppresses T cell proliferation and**
759 **reduces viability *in vitro***. (**A-F**) Naïve T cells isolated from the spleen and lymph nodes of WT or
760 ODC cKO (CD4-Cre, ODC^{fl}) mice were activated by plate-bound anti-CD3 and anti-CD28
761 antibodies with 5 ng/mL IL-2. (**A**), activated WT or ODC cKO T cells were pulsed with BrdU for
762 1 hour before harvest at indicated time points, then stained with intracellular BrdU antibody and
763 DNA marker 7AAD. Cell cycle profile was analyzed by flow cytometry. The numbers indicate the
764 percentage of cells in each cell cycle stage. (**B**), total T cells isolated from WT or ODC cKO mice
765 were stained with cytoplasmic dye CFSE as indicated. Cell proliferation was evaluated by CFSE
766 dilution with flow cytometry. (**C**), the cell cycle profile was evaluated in active T cells in the
767 presence or absence of 2mM DFMO using BrdU (**D**), cell proliferation profile was analyzed for
768 naïve and activated T cells that received either vehicle or 2mM DFMO treatment. (**E-F**), activated
769 T cells under indicated conditions were analyzed for cell viability using 7AAD uptake which
770 indicates the loss of cell membrane integrity, FSC (forward scatter) reflects cell size change. (**A,**
771 **C**) representative of 3 independent experiments, (**B, D, E, F**) representative of 6 independent
772 experiments.

773 **Figure 2. De novo polyamine biosynthesis is dispensable for driving T cell proliferation and**
774 **function *in vivo*.** (**A**), An overview of *in vivo* competitive homeostatic proliferation experimental
775 procedure (left panel). Naïve CD4+ T cells isolated from WT mice (Thy1.1+) and ODC cKO mice
776 (Thy1.2+) were mixed in a 1:1 ratio and stained with CFSE, then adoptively transferred into
777 lymphopenic $Rag^{-/-}$ host mice for *in vivo* homeostatic proliferation. The T cell ratio and proliferation
778 were evaluated in WT and ODC cKO cells by Thy1.1/Thy1.2 cell surface staining and CFSE
779 dilution, respectively, by flow cytometry (right panel). (**B**), An overview of *in vivo* competitive OT-
780 II T cell antigen (ovalbumin/OVA) driven proliferation experimental procedure (left panel). Naïve
781 CD4+ OT-II T cells isolated from WT OT-II mice (Thy1.1+, CD45.2+) and ODC cKO OT-II mice
782 (Thy1.2+, CD45.2+) were mixed in a 1:1 ratio and labeled with CFSE, then adoptively transferred

783 into CD45.1+ host mice, which were immunized in the hock with OVA peptides. After 7 days,
784 popliteal draining lymph nodes were collected, and donor cell ratio and proliferation were analyzed
785 by flow cytometry. Data are representative of 2 independent experiments. (**C**), An overview of
786 induced experimental autoimmune encephalomyelitis (EAE) experimental procedure. Mice with
787 indicated genotypes were immunized with MOG/CFA to induce EAE, and clinical scores were
788 evaluated daily. (**D**), WT mice were immunized with MOG/CFA, and treated with 1% DFMO in
789 drinking water or regular drinking water (vehicle) from day 0 throughout the experiment. Clinical
790 scores were evaluated daily. (**C, D**) EAE data indicate mean ± SEM. N=5. (**A, C, D**) representative
791 of 3 independent experiments.

792 **Figure 3. Ablation of de novo polyamine biosynthesis renders T cells dependent on polyamine**
793 **uptake that can be blocked by AMXT1501.** (**A**), Relative putrescine uptake of naïve and activated
794 T cells was determined by the cellular retention of ^{14}C labeled putrescine. (**B**), relative putrescine
795 uptake of WT and ODC cKO cells after 24 hours activation. (**C-F**), naïve T cells isolated from WT
796 or ODC cKO mice were activated by plate-bound antibodies in presence of 5 ng/mL IL-2. (**C**), Cell
797 cycle profile was evaluated in WT, ODC cKO, and ODC cKO groups supplemented with 3μM
798 polyamine mixture (putrescine 1 μM, spermidine 1 μM, spermine 1 μM) using BrdU after 48hour
799 of T cell activation. The numbers indicate the percentage of cells in each cell cycle stage. (**D**), Cell
800 proliferation was evaluated as indicated condition by CFSE dilution. (**E**), isolated T cells with
801 control vehicle (PBS as solvent) , 2 mM DFMO (ODC inhibitor), or 2 mM DFMO with 3 μM PA
802 mixture treatment were activated, BrdU pulsed, and analyzed for cell cycle profile as described in
803 **C**. (**F**), cell proliferation profile at indicated time point was analyzed for activated T cells in
804 presence and absence of , 2 mM DFMO, or 2 mM DFMO plus 3 μM PA mixture as described in
805 **D**. (**G**), overview of cellular polyamine homeostasis through biosynthesis and uptake as well as the
806 pharmacological inhibitors' function of depleting intracellular polyamine pool (top panel). The
807 effect of DFMO alone or combined with polyamine uptake inhibitor AMXT1501 (1 μM) on

808 polyamine uptake in 24-hour activated T cells was evaluated as described in **A.** (**H**), Cell
809 proliferation profile was evaluated for indicated condition by CFSE dilution. (**A, B, G**)
810 representative of 4 independent experiments. (**C, D, E, F, H**) representative of 3 independent
811 experiments. Bar graphs indicate mean ± SD.

812 **Figure 4. Simultaneous blockage of polyamine uptake and de novo biosynthesis suppresses T**
813 **cell proliferation and function *in vivo*.** (**A**), overview of *in vivo* competitive homeostatic
814 proliferation experimental procedure (top panel). Naïve CD4+ T cells isolated from WT mice
815 (Thy1.1+) and ODC cKO mice (Thy1.2+) were mixed in a 1:1 ratio and stained with CFSE, then
816 adoptively transferred into lymphopenic *Rag*$^{-/-}$ host mice for *in vivo* homeostatic proliferation. Host
817 mice were randomly divided into two groups and treated with vehicle (PBS as control) or
818 AMXT1501 (3mg/kg/day s.c.) for 4 days. Peripheral lymph nodes were collected, and the
819 percentages of WT and ODC cKO cells as well as cell proliferation were analyzed by
820 Thy1.1/Thy1.2 cell surface staining and CFSE dilution by flow cytometry, respectively. (**B**), An
821 overview of *in vivo* competitive OT-II T cell antigen (ovalbumin/OVA) driven proliferation
822 experimental procedure (top panel). Naïve CD4+ OT-II T cells isolated from WT OT-II mice
823 (Thy1.1+, CD45.2+) and ODC cKO OT-II mice (Thy1.2+, CD45.2+) were mixed in a 1:1 ratio and
824 labeled with CFSE, then adoptively transferred into CD45.1+ host mice, which were then
825 immunized in the hock with OVA peptides and treated with vehicle (PBS as control) or AMXT1501
826 (3mg/kg/day s.c.). After 7 days of *in vivo* proliferation, draining lymph nodes were collected,
827 percentage and proliferation of donor cells were analyzed by flow cytometry. (A-B) representative
828 of two independent experiments. (**C**), An overview of induced experimental autoimmune
829 encephalomyelitis (EAE) (top panel). Mice with indicated genotypes were immunized with
830 MOG/CFA to induce EAE. Each sub-group from WT and ODC cKO mice were treated with
831 polyamine uptake inhibitor AMXT1501 (3mg/kg/day s.c.), and clinical scores were evaluated for
832 4 groups daily. Data represents 2 independent experiments. (**D**), The schematic diagram of DFMO

833 and AMXT treatment in EAE model. WT mice were immunized with MOG/CFA, randomized into
834 four groups for the treatment with vehicle (PBS as control), AMXT1501(3mg/kg/day s.c.), DFMO
835 (1% in drinking water), and DFMO (1% in drinking water) + AMXT1501(3mg/kg/day s.c.),
836 respectively, throughout the experiment. Clinical scores were evaluated daily. Data represents 2
837 independent experiments. EAE data indicate mean ± SEM. N among 5 to 10.

838 **Figure 5. Arginine catabolism supports polyamine biosynthesis and T cell proliferation.** (**A**),
839 diagram of $^{13}C_5$-Glutamine, $^{13}C_6$-Arginine, and $^{13}C_5$-Proline entering the intracellular polyamine
840 biosynthesis pathways. (**B**), Naive T cells isolated from spleen and lymph nodes of WT mice were
841 activated by plate-bound method in Gln/Arg/Pro triple-free media supplemented with $^{13}C_5$-
842 Glutamine or$^{13}C_6$-Arginine, or $^{13}C_5$-Proline respectively for 36 hours, extracted, and analyzed for
843 indicated metabolites using CE-TOFMS as described in methods. (**C**), T cell viability in the
844 indicated conditional media at designated time point was determined by 7AAD uptake. (**D**), naïve
845 CD4+ T cells isolated from WT mice were labeled with CFSE, activated, and differentiated in
846 arginine-free RPMI1640 or high-level arginine supplemented (1000μM, which comparable with
847 complete RPMI 1640) media for 72 hours. The indicated proteins IFN-ɣ (T_H1), IL-17 (T_H17), and
848 FoxP3 (iT_{reg}) were quantified by intracellular staining following PMA and ionomycin stimulation.
849 Cell proliferation in arginine-free or high-level arginine supplemented media was determined by
850 CFSE dilution. (**E**), isolated T cells were either maintained in culture media containing 5 ng/mL
851 IL-7 as naïve T cells or activated in the arginine-free conditional media with 5 ng/mL IL-2 and
852 increased concentrations of arginine (0 μM, 10 μM, and 1000 μM), respectively. T cell protein
853 synthesis levels (FITC staining) and cell size (FSC) were evaluated at 24 hours. Cell proliferation
854 (CFSE) and its ability to polarize into T_H17 (IL-17) were evaluated at 72 hours. (**B, E**)
855 representative of 2 independent experiments. (**C**) representative of 5 independent experiments. (**D**)
856 representative of 3 independent experiments. Bar graphs indicate mean ± SD.